

Construction in structural glass: behaviour of Glass-GFRP composite beams

Luís Guilherme da Cunha Seixas Valarinho

Instituto Superior Técnico, Universidade Técnica de Lisboa

Av. Rovisco Pais 1, 1049-001 Lisboa, Portugal

E-mail: luis.valarinho@gmail.com

1. INTRODUCTION

The use of glass with structural functions has attracted a growing interest by the technical community (architects in particular), essentially due to its transparency and numerous aesthetical possibilities. This increased receptiveness from the technical community can be perceived in many contemporary applications of glass in different types of constructions. In fact, besides the increasing non-structural applications, in which glass does not work as load bearing element, solutions in which glass has a greater structural importance, such as beams (Figure 1) or columns (Figure 2), are increasingly common. Nevertheless, when used as structural material, glass presents some disadvantages when compared to traditional materials, most notably the fragile behaviour and the reduced resistance to tensile stresses.



Figure 1 - Use of *glass fins* as support elements of a roof with a span greater than 15 m, Glasgow, Scotland [1].



Figure 2 - Glass columns in a convention center in Saint-Germain, France [2].

In order to overcome the above mentioned disadvantages, the glass industry has developed two improved fabrication methods: (i) glass toughening; and (ii) glass lamination. In the first method, glass is submitted to a thermal treatment that induces compressive stresses in its edges, contributing to the closure of possible flaws and therefore to increase its tensile strength. The underlying principle of the second method, which consists of joining two or more glass panes by PVB foils, relies on structural redundancy – if one glass pane breaks down, the additional panes prevent the collapse and the PVB foils prevent the falling of material. However, neither of these solutions (which can be used concomitantly) eliminates the fragile behaviour of glass, simply allowing to circumvent it.

One of the lines of investigation in the area of structural glass has consisted of developing composite structural solutions, in which glass is associated to other materials, aiming to increase its stiffness and strength and/or guaranteeing more ductile failure mechanisms. Amongst the composite solutions that have been suggested and studied, it is worth mentioning the combination of glass with stainless steel elements, carbon fibre reinforced polymer (CFRP) laminates, concrete, wood and steel (Figures 3 and 4).

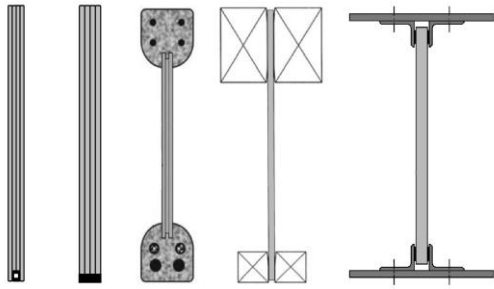


Figure 3 – Composite solutions with glass and (from left to right) stainless steel, CFRP laminates, concrete, wood and steel [3].



Figure 4 – Use of glass-wood composite beams in a conference room [4].

A significant part of the research on composite glass structures has been undertaken at Delft University, and it involves the development of glass-stainless steel composite beams - the aim of the project is the construction of composite beams with the ability to support spans of up to 18 m. Some studies have already been undertaken showing that glass-stainless steel composite beams with spans up to 7.2 m are viable. Aspects such as the effect of the geometry of the cross section [5–7], the geometry of the reinforcement and the type of adhesive [8] have been thoroughly studied, allowing for a better understanding of the behaviour of such composite structures.

Researchers from Delft University have studied several cross section geometries (T, square, rectangular) by bonding glass panes (adjacent or perpendicular to each other) with structural adhesives (Figure 5). Experiments allowed evaluating the susceptibility to lateral-torsional buckling of beams presenting those different cross-sections - with the rising level of cracking throughout the cross-section, the area of glass subjected to compression stresses decreases, thereby increasing the risk of occurrence of this kind of instability phenomenon.

In the investigations about the effect of the reinforcement geometry, researchers from Delft University paid particular attention to the failure modes and the level of ductility achieved by the beams. Despite the positive results obtained for the three types of geometries analyzed (Figure 6), several differences were found in their behaviour. As an example, the geometry 2F (c.f. Figure 6) allowed for a better control of the beam's ultimate failure, since the detachment of one of the reinforcement sections did not lead to the beam's collapse. The geometry 3F, with the reinforcement integrated in the web of the beam and enclosed between glass panes, was the one that showed the best structural behaviour, with a very high degree of ductility and a failure mode that did not involve the detachment of the reinforcement section, but instead the disintegration of the glass web. However, both 2F and 3F geometries involved considerable difficulties in the fabrication process, which had not been found in geometry 1F, for which the reinforcement was far less complex.

The results presented in this paper are based on a study which had the objective of characterizing the mechanical behaviour of the glass material and study the serviceability and the ultimate behaviours of glass structural elements. In addition, experimental and numerical investigations were carried out about structural solutions involving on composite beams combining glass and glass fibre reinforced polymer (GFRP) laminates. The solutions presented in this paper, which can be used in new constructions or in the rehabilitation of existing glass structures, consist of bonding, with different structural adhesives, a web made of annealed glass (keeping the transparency of the structural element) and flanges of GFRP composite material. Besides the increase of stiffness and strength due to the change in geometry, the solution proposed aimed also at obtaining more ductile failure modes, due to the effect of load redistribution from the glass web to the reinforcement elements, and also due to the eventual deformation capacity of the adhesives used in the joints. Besides the experimental tests, the study includes also the development of numerical and analytical models which allowed for a better understanding of the serviceability behaviour of the tested beams.

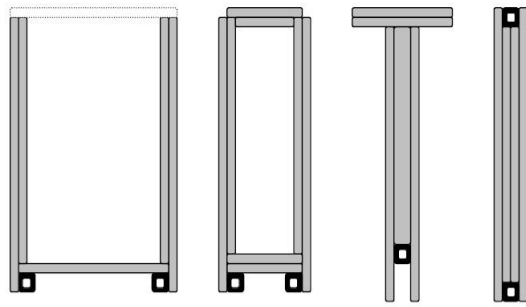


Figure 5 – Geometries of the several cross sections tested at Delft University [3].

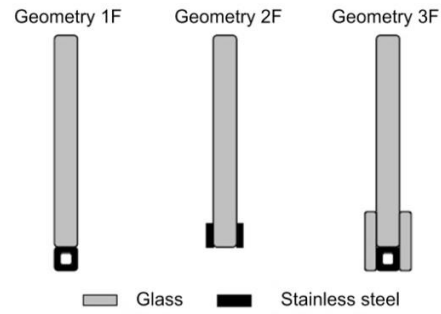


Figure 6 – Different reinforcement sections tested at Delft University [8].

2. EXPERIMENTAL PROGRAMME

2.1 Test programme and objectives

In an initial stage, the experimental program included material characterization tests carried out on small scale specimens, in order to determine the mechanical properties of the materials used: (i) annealed glass, the main material being studied; (ii) GFRP pultruded laminates, used as reinforcement material; and (iii) three different structural adhesives – polyurethane, epoxy and acrylic, used to connect the two previous materials.

Subsequently, double lap joints between glass and GFRP laminates were manufactured and tested in tension. These tests allowed comparing the three types of adhesives mentioned, regarding the ease of application and the serviceability and ultimate behaviour of the joints.

Finally, 4-point bending tests were carried out on annealed glass beams and on glass-GFRP composite beams, all simply supported. These tests allowed analyzing the serviceability and ultimate behaviour of both types of solutions and, particularly, allowed evaluating the advantages of the suggested composite solutions.

2.2 Materials

Throughout the experimental campaign, 12 mm thick annealed glass panes with edge treatment, provided by Guardian, were used. The use of tempered glass was not considered adequate for this study, since the increase in tensile strength would originate, simultaneously, a decrease in the residual integrity after initial cracking. Four-point bending tests were carried out (Figure 7), according to EN 1288-1,3 standard [9], to characterize the ultimate strength of glass. The elasticity modulus in bending of the glass was determined in the flexural tests of the glass beams. In both types of tests, glass presented linear elastic behaviour until failure, with an elasticity modulus in bending of $E_{\text{glass}} = 80.6 \text{ GPa}$ (for the glass beams) and an ultimate tensile stress of $\sigma_u = 58.9 \pm 12.6 \text{ MPa}$ (for the glass laminates).

As reinforcement material, rectangular and angle GFRP pultruded profiles, provided by STEP, were used – both profiles are composed of an isophthalic polyester matrix reinforced with alternating layers of E-glass rovings and mats. The mechanical characterization tests of the rectangular profiles were done by Correia [10] and involved tensile, compressive, flexural and interlaminar shear tests (Figure 8). The main results obtained in those tests are shown in Table 1, namely the ultimate stress (σ_u), the elasticity modulus (E), the ultimate strain (ϵ_u) and the Poisson's ratio, for the different types of loading.



Figure 7 – Flexural tests in annealed glass panes.

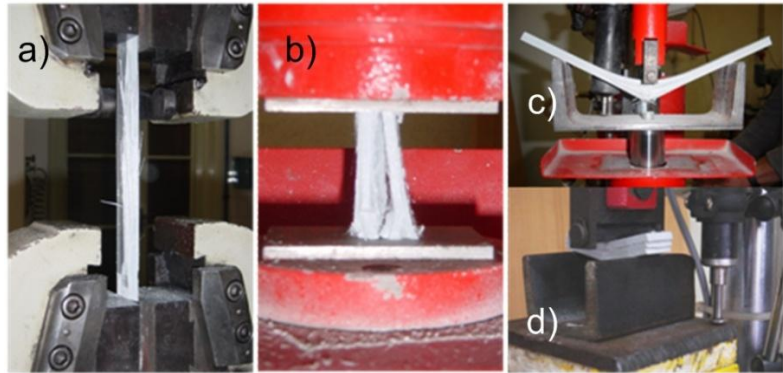


Figure 8 – Specimens of GFRP profiles under a) tensile, b) compressive, c) flexural and d) interlaminar shear testing (adapted from [10]).

Table 1 – Mechanical properties of the GFRP material (adapted from [10]).

Mechanical property	Flexural	Tensile	Compressive	
	Longitudinal	Longitudinal	Longitudinal	Transverse
σ_u [MPa]	624.6 ± 26.9	475.5 ± 25.5	375.8 ± 67.9	122.0 ± 15.4
E [GPa]	26.9 ± 1.3	32.8 ± 0.9	26.4 ± 1.9	7.4 ± 0.4
ϵ_u [10^{-3}]	24.9 ± 1.3	15.4 ± 1.5	17.0 ± 2.5	21.5 ± 1.7
ν_{xy} [-]	-	0.28	-	-

As connection material, the following types of structural adhesives were used: (i) polyurethane (Sikaflex 265), (ii) epoxy (Sikadur 330) and acrylic (Delo Photobond 468), the first two provided by SIKA and the last one by DELO. Both the polyurethane and the epoxy adhesives were submitted to tensile tests, carried out according to ISO 527 standard [11], in order to determine their mechanical properties (Figure 9). It was not possible to do such tests on the acrylic adhesive given the lack of available material. The polyurethane adhesive exhibited a typical elastomeric behaviour, presenting several different phases in its load-deflection curve and a very high deformation capacity (Figure 10). This adhesive presented an initial elasticity modulus of $E_t = 1.49$ MPa; it was not possible to evaluate accurately its average ultimate stress (only one specimen failed, for a maximum tensile stress of $\sigma_{tu} = 3.1$ MPa), because the gripping system did not allow to keep with the significant transverse contraction suffered by the specimens. The epoxy adhesive showed linear elastic behaviour until failure (Figure 11), with an elasticity modulus of $E_t = 5.13$ GPa and an ultimate stress of $\sigma_{tu} = 22.46$ MPa.



Figure 9 – Tensile tests in structural adhesives.

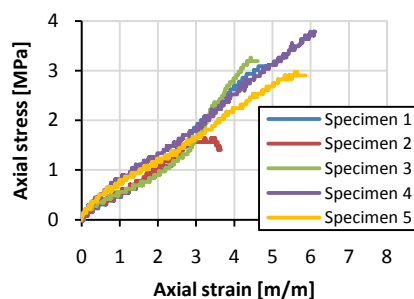


Figure 10 – Axial stress vs. strain curves of PU adhesive specimens.

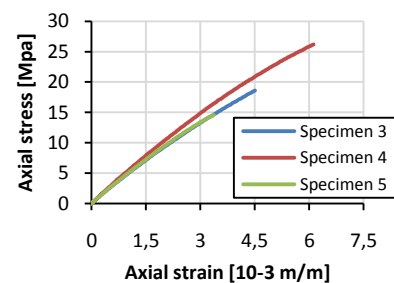


Figure 11 – Axial stress vs. strain curves of EP adhesive specimens.

3. TESTS ON DOUBLE LAP JOINTS

3.1 Specimens description and test setup

The experiments on double lap joints composed of glass and GFRP consisted of tensile tests in specimens constituted by four layers of material: two inner GFRP layers, in whose extremities a tensile load was applied; and two outer glass layers bonded to the former layers using the three different structural adhesives. These tests were conducted to assess the adhesion capacity of the different adhesives in glass as well as in GFRP. They were also useful as a means for having a first contact with the adhesives, their application method and their behavior.

The geometry of the test specimens is illustrated in Figure 1. GFRP profiles and glass panes with a cross section of 10 × 50 mm and 12 × 50 mm, respectively, were used, both with a length of 350 mm. An overlap length of 100 mm was defined – therefore, specimens had a total length of 850 mm. The joint thickness of 2 mm, used in all adhesives, was guaranteed through the placement of rectangular PVC spacers, positioned in 4 points and, occupying no more than 1% of the bonding area.

A total of 10 specimens were tested (Figure 13), distributed by 3 series, with the following designations: PU-[i], EP-[i] and AC-[i], for the specimens made from the polyurethane (4 specimens), epoxy (3 specimens) and acrylic (3 specimens) adhesives, respectively. Tests were carried out in a universal Instron testing machine, at a load speed of 0.017 mm/s (displacement between grips). During the test the applied load and the displacement of the specimen in the overlap zone were measured - for this purpose, two TML displacement transducers, model CDP-500, were placed in both sides of the test specimens. All specimens were wrapped in cellophane film, with the objective of preventing the dispersion of glass fragments in the machinery or in the laboratory after the specimen failure.



Figure 12 – Geometry of the specimens used on double lap joint tests: section view (top) and detail of the overlap zone (bottom).

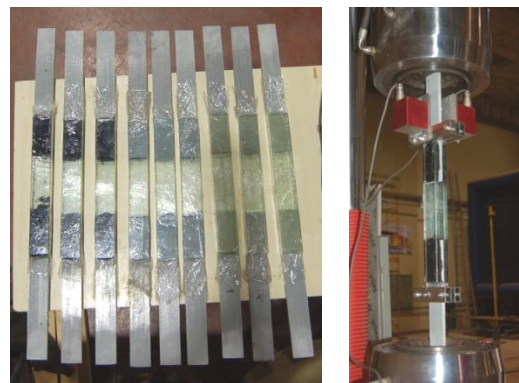


Figure 13 - Double lap joint tests: general view of all specimens (left) and of test setup (right).

3.2 Results and discussion

3.2.1 Application process

After bonding all specimens, and still before the beginning of the tensile tests, some conclusions could be drawn about the ease of application of the adhesives. About the polyurethane adhesive, it is worth highlighting its black colour, mode of application by sealant gun and high viscosity, which made the application process more difficult; additionally, during the curing process, this adhesive suffered considerable volumetric changes and it was also noticed that air bubbles appeared in the bonding area. The epoxy adhesive showed fluidity and ease of application (by spatula); after the curing process, this adhesive presented high hardness, only allowing changes to be made to its finishing by means of mechanical processes. In what concerns the acrylic adhesive, it is worth mentioning its curing process, which only developed when subjected to ultraviolet light

(UV); apparently, the lack of suitable equipment for this process and the opacity of the GFRP reinforcement did not allow for an appropriate curing of this adhesive.

3.2.2 Load-displacement response and failure modes

Figure 14 presents the load vs. displacement curves of the PU, EP and AC series and Figure 15 illustrates the failure modes for each type of adhesive tested.

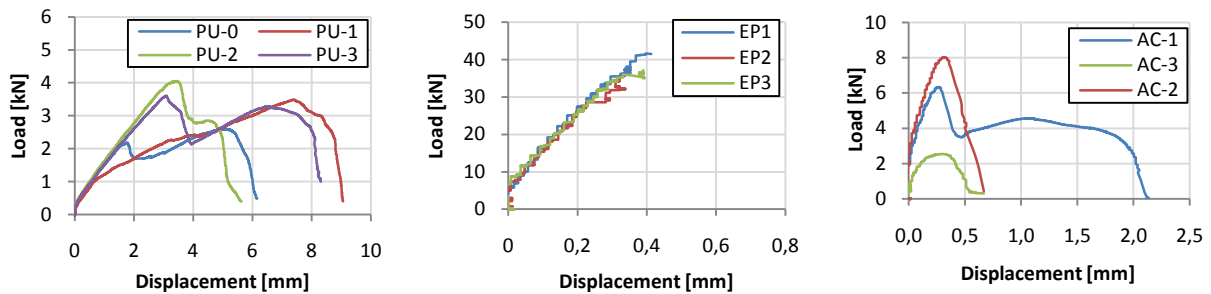


Figure 14 – Load vs. displacement curves of the PU, EP and AC series (from left to right).

Specimens of PU series presented an initially linear behaviour; however, for relatively low loads, the specimens showed a progressive stiffness reduction, presumably due to the detachment amongst adherents. On the other hand, the behaviour exhibited by the several specimens was somewhat distinct, some of them showing significant stiffness reduction – this behaviour, associated to the relative slipping between the pieces of the joint, is related to the previously mentioned adhesive problems, namely the difficulties found out in the application process.

Specimens of AC series also presented non-linear behaviour and, by comparison with the PU series, the pattern of the load vs. displacement curves showed a smaller variability until failure; however, a higher dispersion was verified in the maximum load values (mostly due to the apparently anomalous behaviour of one of the specimens). All specimens of PU and AC series presented adhesive failure, with the slippage between materials having caused the total separation of the pieces bonded.

Specimens of EP series presented a practically linear behaviour until failure, without significant changes in stiffness, showing that the quality of the connection did not suffer any degradation. This result is also proven by the fact that failure of all specimens occurred in the glass panes, under tensile stress, which demonstrates the stress transfer capacity of this kind of joint.

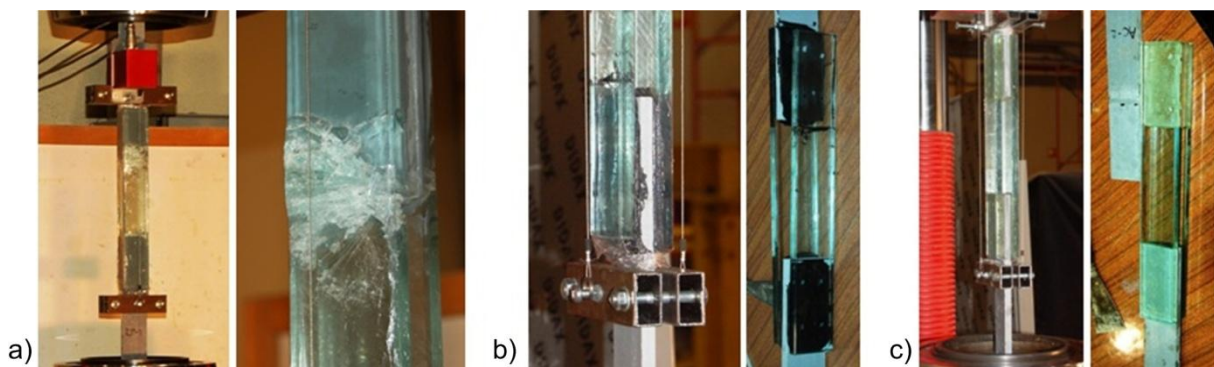


Figure 15 – Double lap joints failure modes for a) epoxy, b) polyurethane and c) acrylic adhesives.

3.2.3 Summary and adhesive selection

Table 2 presents a comparison of the different experimental series, concerning stiffness (K), maximum load (F_{max}), relative corresponding displacement (d_{max}) and failure mode.

Table 2 – Summary of the results obtained in double lap glass-GFRP joints.

Adhesive type	k [kN/mm]	F_{max} [kN]	d_{max} [mm]	Failure mode
Poliurethane	1.08 ± 0.34	3.55 ± 0.61	5.79 ± 1.31	Adhesive
Epoxy	91.86 ± 5.83	37.58 ± 3.38	0.48 ± 0.24	Stock-break (glass adherend in tension)
Acrylic	18.71 ± 3.78	5.63 ± 2.82	0.44 ± 0.09	Adhesive

The joint with polyurethane is characterized by the lowest values of stiffness and strength, with the maximum load corresponding to very high values of displacement, essentially due to the very high deformation capacity of the adhesive and, in addition, to the slippage observed at the adhesive-adherend interfaces. Conversely, the adhesive based on epoxy resin provided strength about 10 times higher than that achieved with the polyurethane adhesive, simultaneously guaranteeing high stiffness, with very low maximum displacements. The specimens with acrylic adhesive showed intermediate results – in terms of stiffness, the values approach those obtained for epoxy adhesive; however, as far as strength is concerned (it is worth mentioning that this was the series where variability was the highest), the results approach those obtained with the polyurethane adhesive.

As for the construction process, all the adhesives proved to be applicable to the construction of glass-GFRP composite beams. The epoxy adhesive presented an excellent workability during the fabrication process, which allowed for excellent finishing; the greatest disadvantage of this adhesive has to do with the hardness acquired after the curing process, which makes the execution of subsequent changes quite difficult. The acrylic adhesive presented a not very adequate curing process for the laboratorial conditions available, which probably was the cause for the considerable dispersion of the results. For the polyurethane adhesive, the main disadvantages consisted of the high viscosity and the significant volumetric changes.

Thus, it was concluded that the epoxy adhesive is the one presenting the best characteristics, both physical (relevant in the application stage) and structural. Notwithstanding, since one of the objectives of this study was the development of composite beams with a ductile behaviour, it was considered interesting to use also the polyurethane adhesive in the beam tests. In fact, despite the aforementioned disadvantages, it was considered that the high deformation capacity (and reduced stiffness) of this adhesive could contribute to increase the beam's ductility. It should be noted that for the epoxy adhesive, given its high stiffness and linear behaviour, the ductility could only be provided by the distribution of loads between glass and GFRP reinforcement (pseudo-ductility).

4. FLEXURAL TESTS ON GLASS AND GLASS-GFRP COMPOSITE BEAMS

4.1 Properties and fabrication of the composite beams

A total of 8 beams, with a length of 1.80 m, were tested in bending, distributed in 3 series: (i) 4 glass beams (S series), (ii) 2 glass beams reinforced with a GFRP pultruded laminate in the bottom edge (R series) and (iii) 2 beams with I geometry, composed of glass webs and GFRP flanges (I series). In the composite beams (series R and I), the connection between glass and GFRP was done with polyurethane adhesive (beams R-PU and I-PU) and epoxy adhesive (beams R-EP and I-EP).

The glass beams consist of an annealed glass pane with section of $100 \times 12 \text{ mm}^2$.

The rectangular beams are constituted of two independent pieces: an annealed glass pane with section of $100 \times 12 \text{ mm}^2$, and a rectangular GFRP profile with section of $12 \times 10 \text{ mm}^2$. The I beams are constituted of

seven independent pieces: an annealed glass pane with section of $100 \times 12 \text{ mm}^2$, four GFRP angles with $30 \times 20 \times 4.8 \text{ mm}^3$ and two rectangular GFRP profiles with section of $76 \times 10 \text{ mm}^2$. All the pieces were bonded with a 2 mm thick layer of adhesive – either epoxy or polyurethane (Figure 16).

Before bonding, all surfaces to be in contact with the adhesive were polished with sandpaper (for the GFRP material) and cleansed of grease with acetone. To ensure a constant thickness of the adhesive layer, 2 mm thick PVC spacers were used. The fabrication process of both reinforced beams basically consisted of bonding all constituting elements. For the rectangular beams, the process took place in a single stage; for the I shaped beams, the process was developed in four stages (Figure 17), given the number and relative position of pieces to bond. A time delay of 24 h was set between stages, considered to be enough for achieving a partial curing of the adhesives, thereby allowing to move beams safely. In all stages there was particular care with the cleaning and finishing of the adhesive layer.

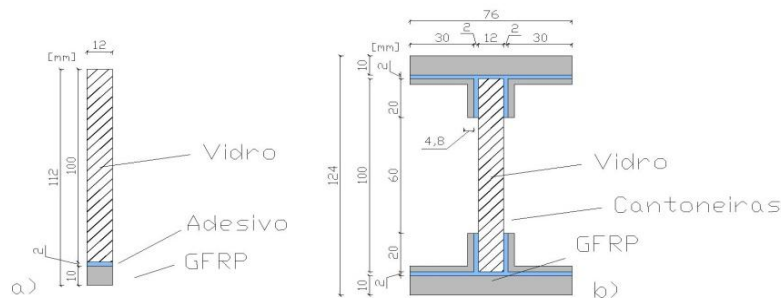


Figure 16 – Geometry of the glass-GFRP composite beams: rectangular section (left) and I section (right).

4.2 Experimental setup and test procedure

All beams, with a length of 1.80 m, were tested under 4-point bending in a span of 1.50 m (Figure 18). For series S and R, in order to prevent eventual lateral displacements small metallic guides were placed in the supports, together with two pairs of vertical metallic bars positioned along the span at a distance of 72.5 cm. The load was applied by means of an Enerpac hydraulic jack, with a load capacity of 100 kN, and metallic distribution beams. On S and R beams, two small rubbers were placed under the load points in order to avoid glass-metal contact. Load was measured with a Novatech load cell, with a load capacity of 300 kN. The mid-span displacements were measured with electrical TML displacement transducers, with strokes of 25 mm and 50 mm. On R and I beams, the axial strain at different heights of the mid-span section were measured with electrical TML strain gauges. Before the tests, all beams were wrapped in cellophane film to prevent the dispersion of fragments of broken glass. The beams were monotonically loaded until failure, in load control, and the recording of load, displacement and strains values was done in PC, by means of a 100 channel data acquisition unit from HBM, model UPM100.



Figure 17 – Different stages of I section composite beams fabrication process.

4.3 Results and discussion

The load vs. displacement curves of the tested beams are presented in Figure 19 (for S series, only one curve, which is representative of the remaining beams, is presented).



Figure 18 – Experimental setup for the bending tests (beam I-PU).

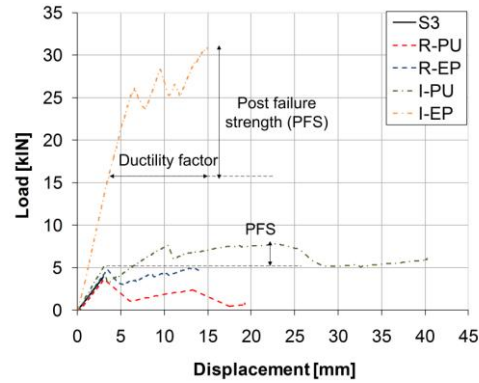


Figure 19 – Load vs. displacement curve for composite beams.

As expected, the annealed glass beams showed linear behaviour (with constant bending stiffness in all beams) until failure, which happened in a sudden and fragile mode, due to the appearance of cracks (generally, a single crack in the central zone), which led to the collapse of the beam.

In beam R-PU, in a first stage, the behaviour was also linear, with a bending stiffness similar to that of beams S. For a load of 3.6 kN (also similar to the strength of those beams), a sudden and significant load reduction occurred, which corresponded to the first visible crack in the glass. From this instant until the end of the test, the load vs. displacement curve shows a set of linear segments, with successive stiffness reductions and one additional sudden load decrease. On those several segments, in which the cracking of one of the cracks progressed considerably, the beam was able to recover a part of the maximum load reached in the previous segment, without ever re-attaining the maximum load corresponding to the first crack. The beam was unloaded, without having failed completely, when mid-span displacement was 19.3 mm (the displacement transducer had reached its limit).

Beam R-EP showed a load-displacement behaviour that was qualitatively similar to that of beam R-PU. In fact, until the appearance of the first visible crack and until the consequent applied load reduction, the beam showed also linear behaviour - however, the bending stiffness was greater than that of beams S and R-PU. On a second stage, as with beam R-PU, the load-deflection curve of beam R-EP presents several linear segments, separated by small load reductions, in which successive decrease of bending stiffness is observed. However, in this beam, and contrarily to beam R-PU, the load decreases in this stage were less significant, and the maximum load attained (4.94 kN) actually reached the value corresponding to the first visible crack in the glass (4.75 kN). During this stage, the propagation and increase in cracking were clear all over the beam, namely towards the supports (Figure 20). The failure of the beam eventually occurred by shear, next to one of the supports, for a mid-span displacement of 13.8 mm.

Beam I-PU showed linear elastic behaviour until a load of 5.1 kN, for which the appearance of the first crack in the glass was visible, giving rise to a sudden load reduction. The beam kept its integrity and actually was able to achieve a considerable load recovery, which increased up to 7.5 kN. This load increase occurred with a progressive decrease in bending stiffness, accompanied by the growth of one of the cracks. The following portion of the load-displacement curve was non-linear and an approximately horizontal plateau occurred for a load of about 7.8 kN. When the mid-span displacement reached a value of about 23.0 mm, the increase in relative slippage between the lower flange of the beam and the glass web became visually perceptible. This corresponded to a gradual load reduction, which only stabilized at a value of 5.0 to 6.5 kN. The beam was unloaded without failing (although the web was significantly cracked), for a mid-span displacement of 40.2 mm (Figure 21).

Beam I-EP showed linear behaviour up to a load value of 15.5 kN, at which the first visible crack developed, precisely at mid-span. This crack is perceptible in the load vs. displacement curve, only due to the slight

stiffness decrease - unlike the previous beams, no load decrease occurred at this stage. Then, in parallel with the cracking progression, the load continue to increase, approximately linearly, until reaching the value of 26.0 kN, for a midspan deflection of 6.5 mm. At this point the first load reduction occurred, but the beam did not loose its integrity– at this instant, in a sudden way, a practically horizontal propagation of the cracks towards one of the supports happened. In the following segment of the load-deflection curve, the beam linearly recovered the load reduction, having even attained a new maximum load of about 28 kN – a load decrease then occurred, corresponding to a similar propagation of the cracks toward the other support (Figure 22). Subsequently, after short segments of load increase and posterior load reduction, the beam presented a non-linear behaviour until failure, which happened in a sudden way, by explosive disintegration of the glass web, for a load of 30.8 kN and a midspan deflection of 15.0 mm.



Figure 20 – Beam R-PU: crack propagation before ultimate failure.



Figure 21 – Beam I-PU: deformation and overview of crack propagation before unloading.



Figure 22 – Beam I-EP: crack propagation before ultimate failure.

The readings of the strain gauges allowed to asses (i) the interaction degree provided by the two types of adhesives and (ii) the distribution of stresses between glass and GFRP during the glass cracking process. On the two beams constituted by the polyurethane adhesive (R-PU and I-PU – Figure 23), even for reduced levels of load (including before the first visible crack appeared), significant slippage occurred (partial interaction) in the interface zones – Bernoulli's hypothesis therefore was not verified. Even so, in beam I-PU, the adhesive was able to distribute some of the stresses on the reinforcement material, evidenced by the increase of axial strains and curvature in the GFRP (by comparison with the behaviour exhibited before the cracking of the glass, for identical load levels). On the beams with epoxy adhesive (R-EP and I-EP – Figure 24), until the beginning of glass cracking, the instrumented sections remained plane, a complete interaction amongst the materials joined by the adhesive was therefore verified. When the glass cracking process started to evolve, a very significant increase of strains in the lower GFRP reinforcement was verified – such strain increase was not followed by the glass and corresponded precisely to the desired distribution of stresses. The connection with epoxy adhesive kept, at this stage and for increasing load levels, enough stiffness and strength to guarantee an adequate redistribution of stresses between the glass and the GFRP.

Table 3 shows a summary of the results obtained in the flexural tests, namely the load associated with the first crack, the maximum load, the post-failure strength (ratio between the load associated with the first visible crack and the maximum load after initial crack), the mid-span deflection (δ) associated with the first visible crack, the midspan deflection at 80% of the maximum load, the deflection at failure and, finally, the ductility factor (ratio between the mid-span deflection associated with the first visible crack and the deflection at failure) and the corrected ductility factor (in which the deflection at 80% of the maximum load was considered instead of the deflection at failure). The values listed in Table 3 show that the greatest ductility indexes correspond to beams with I geometry, particularly with polyurethane adhesive. It can also be seen that, for both beam reinforcement geometries, the highest ductility values occurred together with a significant decrease of initial strength and post-failure strength.

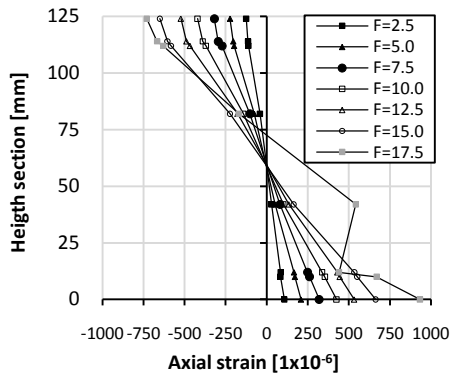


Figure 24 – Beam I-EP: axial strains vs. section height for different load values, in kN (F = 17.5 kN after initial failure).

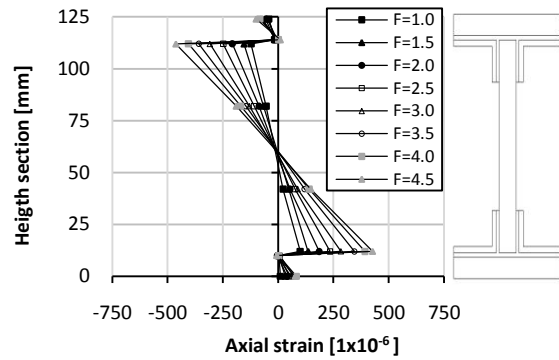


Figure 23 – Beam I-PU: axial strains vs. section height for different load values, in kN (before initial failure).

Table 3 – Summary of the 4-point bending tests results.

Beam type	S	R-PU	R-EP	I-PU	I-EP
Initial failure load [kN]	3.74 ± 0.49	3.6	4.75	5.09	15.50
Maximum load [kN]	3.74 ± 0.49	3.6 ¹	4.94	7.80 ¹	30.81
Post-failure strength [%]	0%	67%	104%	156%	199%
δ on the first visible crack [mm]	2.92 ± 0.35	3.03	3.5	3.0	3.5
δ at 80% of maximum load	-	13.27	-	26.5	-
δ on failure [mm]	2.92 ± 0.35	19.3 ¹	13.8	40.3 ¹	14.9
Ductility factor [%]	0%	537%	294%	1243%	326%
Corrected ductility factor ² [%]	-	338%	294%	783%	326%

¹ Value that did not correspond to the collapse of the beam

² Factor calculated using the δ at 80% of maximum load

5. NUMERICAL INVESTIGATIONS

5.1 Description of the finite element model

Three-dimensional (3D) numerical models of the glass and of the glass-GFRP composite beams were developed (Figure 25), with the objective of simulating and analyzing the serviceability behaviour of the beams tested. All beams were modelled using finite element program ANSYS [12]. The 8-node 3D element SOLID185 was used, with three degrees of freedom per node (translations in directions x, y and z), which allows modelling orthotropic materials and materials with non-linear behaviour. All beams were modelled with the same geometry of the tested beams.

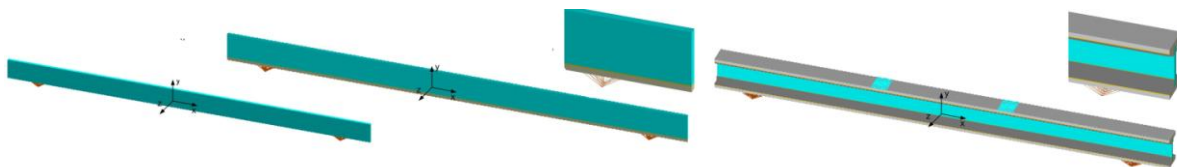


Figure 25 – 3D perspective of the (from left to right) glass beam, rectangular beam and I section beam.

The mesh was manually defined – only “brick” elements were used (instead of pyramidal), as they allow obtaining better results. The mesh created in all beams was obtained by dividing the several material blocks across their thickness: (i) all adhesive blocks were divided in 3 layers; (ii) all GFRP laminates were divided in 2 or 3 layers; and (iii) the glass material, which is significantly thicker than the previous two, was divided in 10

(for the glass and rectangular beams) or 24 layers (I section beams). All other divisions were made in such a way that all dimensions of the elements were smaller than 10 mm.

The numerical modelling of the supports and the applied loads was carried out in order to simulate as faithfully as possible the actual experimental conditions - both the loading and supporting zones were defined as being distributed through an area corresponding to that occupied by the respective metal plates and roller supports used in the tests, thereby avoiding the development of excessive (inexistent) stress concentrations. Applied loads were defined as surface loads at the top surface of the beams – these were applied in the finite elements located below the metallic plates used in the tests (Figure 26, left). For the supports, in order to accurately reproduce the displacements and rotations restraints of the tests, rigid one-dimensional *bar elements* were used. These bars connected extra nodes, in which the beam supports conditions were defined (drawn in a position corresponding to the centre of the rollers used in the experiments), and all nodes from the bottom surface of the beam located in the support zone (in particular, those positioned above the metal plates of the supports) - Figure 26.

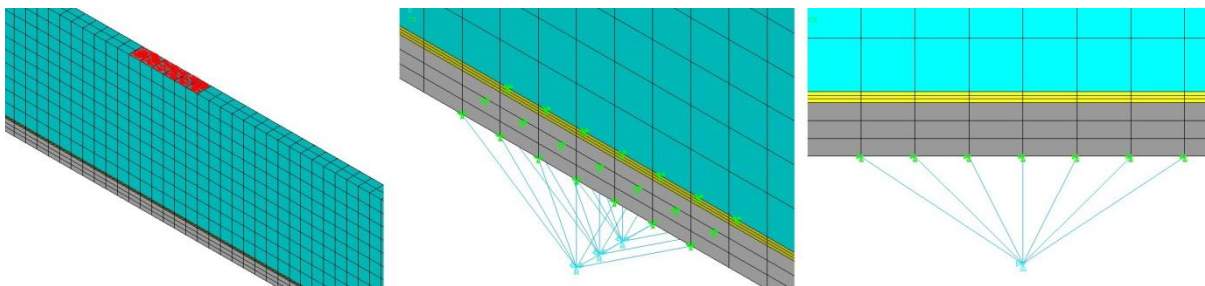


Figure 26 – Finite element model of the (from left to right) application load zone and supporting zone.

All beams were modelled as simply supported, with the corresponding nodal restrictions having been defined in the above mentioned extra nodes. An additional restriction was also defined at the beams mid-span, in which deflections in the direction transverse to the plane of the beam were prevented.

The models did not include the sliding at the interfaces (which had been observed in some experiments, particularly in specimens with polyurethane adhesive), due to the lack of information (as an example, friction coefficients were not known). Therefore, any partial interaction at the bonded interfaces (such as that observed in the beams with polyurethane adhesive) would have to result from the adhesive deformation.

All beams were subjected to a static linear elastic analysis.

5.2 Material properties

The three different types of materials (glass, GFRP and structural adhesives) used in the beams were modelled and their individual mechanical properties were taken into consideration:

- the GFRP was modelled as orthotropic material with linear elastic behaviour;
- the glass was modelled as isotropic material with linear elastic behaviour;
- all adhesives were modelled as isotropic materials with linear elastic behaviour.

For the GFRP, a distinction was also made between the rectangular profile used as reinforcement on the top and bottom edges of the glass panes and the angle profile used to increase the bonding area between the flanges and the web - some of their mechanical properties were differentiated, namely the elasticity modulus. Regarding the adhesives, besides the distinction in their physical behaviour, the mechanical properties were modelled taking into account the results obtained in the material characterization tests, presented in section 2.2. For the modelling of the supports, namely the rigid bars, a very stiff material was considered, with an

elasticity modulus of $E_t = 210 \times 10^7$ GPa. The mechanical characteristics considered for all materials are summarized in Tables 4 and 5.

Table 4 – Mechanical characteristics of GFRP, glass and rigid material used in the FE models.

Características	Reforço	Cantoneira	Vidro	Material rígido
E_x [GPa]	32.8	19.7	80.6	210×10^7
E_{yt} [GPa]	3.5	3.5	-	-
E_z [GPa]	8.5	8.5	-	-
ν_{xy}	0.3	0.3	0.2	0.3
ν_{yz}	0.09	0.09	-	-
ν_{xz}	0.09	0.09	-	-
G_{xy} [GPa]	3.6	3.6	-	-
G_{yz} [GPa]	3.6	3.6	-	-
G_{xz} [GPa]	3.6	3.6	-	-

Table 5 – Mechanical characteristics of the adhesives used in the FE models.

Características	Adesivo PU-1	Adesivo PU-2	Adesivo EP
$E_{x,e}$ [MPa]	1.48	586	5137
$E_{x,p}$ [MPa]	-	31	-
ν_{xy}	0.42	0.42	0.37
$\sigma_{x,ced}$ [MPa]	-	15	-

5.3 Model validation

In order to verify the reliability of the numerical models developed, the experimental mid-span deflections of the beams tested (δ Experimental) were compared with results obtained from numerical models (δ Modeled) and analytical formulae¹ (δ Analytical) - analytical deflections were determined only for the glass and rectangular beams. The summary of such comparison is presented in Table 6. It can be seen that results obtained with the numerical models do not differ more than 13% from experimental data. In addition, it is worth mentioning that for the glass and EP beams, the displacements obtained in the numerical models are lower than those measured in the experiments, while for the PU beams, experimental deflections are higher than numerical predictions.

Table 6 – Comparison between experimental, numerical and analytical results

Applied load		F=2.5 kN			F=4.5 kN	
Beam		Glass	R-PU	R-EP	I-PU	I-EP
δ Numerical	[mm]	1.867	2.229	1.625	3.006	0.987
δ Experimental	[mm]	1.921	2.191	1.844	2.655	1.099
$\Delta 1$	[%]	-2.8%	1.7%	-11.9%	13.2%	-10.2%
δ Analytical	[mm]	1.858	1.612		-	-
$\Delta 2$		0.5%	38.3%	0.8%	-	-

¹ Value obtained from S3 beam, considered representative of the glass specimens tested.

According to the finite element method theory, one would expect that the numerical model, developed based on displacements approximations, would provide conservative results for deflection measurements - this was observed in the glass beams and in the reinforced beams with epoxy adhesive. The fact that non-conservative estimates were obtained for the reinforced beams with polyurethane adhesive may be associated with the variability in the material properties and, eventually, to the error involved in the several tests undertaken, which may have influenced more significantly this type of beams. However, taking into account the results presented it is plausible to admit that the numerical models represent with relative high precision the beams tested. This conclusion is also attested by the similarity with analytical results, particularly

¹ The analytical results were obtained based on the standard theory used in the design of steel-concrete composite structures, but considering a beam constituted by glass and GFRP and taking into account the following hypothesis: (i) inexistence of relative slippage between the two materials (full connection and interaction) and (ii) validity of Bernoulli's hypothesis.

for the glass beams and the reinforced beams with epoxy adhesive. As discussed next, differences observed for the beams with polyurethane stem from the very high deformations exhibited by this adhesive – a full interaction at the interface was not guaranteed.

Figure 27 plots the normal stress distributions at midspan for the glass beam and the beams with epoxy adhesive, in which a full interaction was observed at the interfaces, for loads of 2.5 kN. Figure 27 shows that the general behaviour of the beams is in agreement with the theoretical assumptions often made for simply supported beams loaded under 4-point bending.

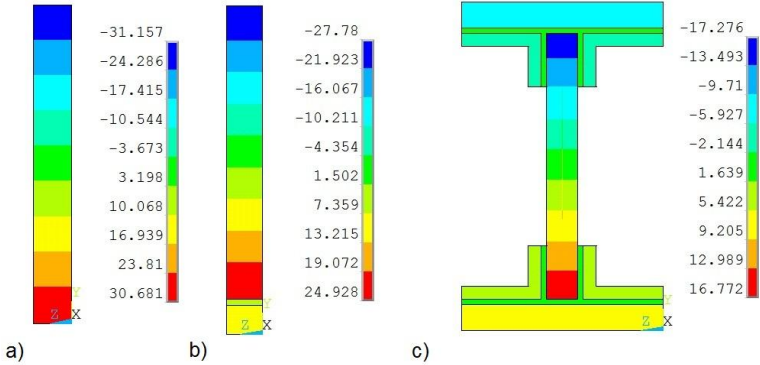


Figure 27 - Normal stress distribution at mid-span of a) glass beam, b) R-EP beam and c) I-EP beam.

5.4 Results

The numerical models developed allowed to analyse the value of the failure stress of the glass in the several tested beams – Table 7. Regarding the obtained data, the failure stress of glass is seen to approach an average value of 50 MPa, which is 9 MPa lower than the value measured in the material characterization tests. However, one should take into account the aspects that give rise to the variability of the failure stress of glass, namely the dimension of the element and the high scatter obtained in consecutive tests [13].

Table 7 – Values of failure stress of glass in all tested beams.

Beam	S	R-PU	R-EP	I-PU	I-EP
$\sigma_{u, \text{glass}}$ [MPa]	49.955	43.476	49.754	51.910	59.261

The numerical models also showed that the value of the failure stress of glass obtained in the beams with polyurethane adhesive is different from that obtained in the beams with epoxy adhesive. This fact was once again attributed to possible cumulative errors in the experiments and, in addition, to the already mentioned scatter in material properties.

Table 8 lists the maximum stresses observed in the different materials of all reinforced beams. Regarding the stress distribution throughout the different materials of the cross-section, the data obtained from the numerical models allowed concluding that the beams with polyurethane adhesive present a less efficient stress distribution. As a consequence, stresses in the glass are higher than those in the corresponding beams with epoxy adhesive (for the same load level). This difference in the stresses distribution stems from the reduced value of the polyurethane adhesive stiffness, which reduces its efficiency in transferring stresses to the GFRP flange(s).

The axial strains calculated with the numerical models were compared with those measured throughout the midspan section of the tested beams. Table 9 presents the comparison between the numerical axial strains at the interface level (lower interface, in the case of I beams) amongst the two materials and the corresponding experimental data. The data listed in Table 9 shows that, in opposition to data from Table 6, the numerical model presented a lower stiffness (determined from strains) when compared to the experimental results. This

difference may eventually be due to possible errors in the experimental measurements of deformations, caused during the bonding of the strain gauges or due to material defects. In addition, since the approximation of the numerical models is done in displacements, the results obtained for the deformation distributions have lower quality when compared with displacement fields.

Table 8 – Distribution of stresses through the various materials in all modelled composite beams.

Applied load		F = 2.5 kN		F = 4.5 kN	
Beam		R-PU	R-EP	I-PU	I-EP
σ_{glass}	[MPa]	28.556	24.771	43.258	16.360
σ_{GFRP}	[MPa]	2.054	10.777	0.640	6.806
σ_{adhesive}	[MPa]	1.741×10^{-4}	1.566	-1.175×10^{-3}	1.007

Table 9 – Comparison between numerical and experimental axial strains.

Material	ϵ on glass [1×10^{-6}]			ϵ on GFRP [1×10^{-6}]			
	Analysis type	Numerical	Experimental	Δ	Numerical	Experimental	Δ
R-EP		298	300	-1%	329	312	5%
I-EP		195	160	22%	208	168	24%
R-PU		344	332	3%	63	110	-43 ¹
I-PU		516	470	10%	19	7	13 ¹

¹ Absolute value

A qualitative comparison of the axial strains distribution throughout the mid-span section of all analyzed beams was also done (Figures 28 and 29). In general, the curves obtained allow concluding that for the glass-GFRP composite beams with epoxy adhesive Bernoulli's hypothesis is observed, while for the beams with polyurethane adhesive such hypothesis is not verified. In fact, since the numerical model shows the existence of slipping at the interfaces of beams with polyurethane adhesive, it is demonstrated that this phenomenon is due, in a great extent, to the mechanical characteristics of the connection (provided by the adhesive) and not so much by the adhesive adhesion characteristics – this information was not possible to obtain with the experimental data. However, once again, it is worth mentioning the very good agreement between experimental data and numerical results for all tested beams.

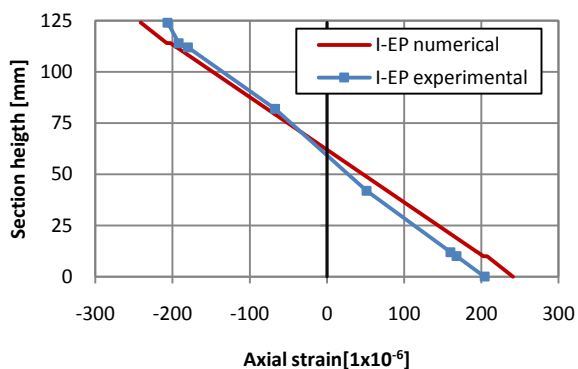


Figure 28 – I-EP beam: numerical and experimental axial strains at midspan section (applied load 4.5 kN)

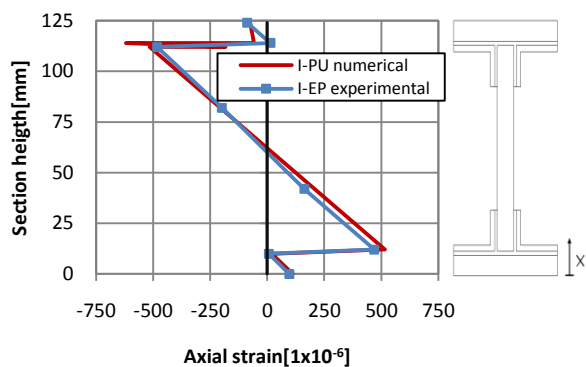


Figure 29 - I-PU beam: numerical and experimental axial strains at midspan section (applied load 4.5 kN).

6. CONCLUSIONS

The tests done proved the advantages and technical viability of the use of glass-GFRP composite beams. In particular, it has been proven that a safe and relatively ductile failure mode of glass elements can be obtained through their bond to GFRP profiles. In fact, after the first crack, all the GFRP reinforced beams kept their integrity, remaining with a residual resistance capacity, which varied with the type of adhesive and, as expected, with the geometry of the reinforcement. In addition, the composite solutions allowed increasing both stiffness and strength.

From a resistance standpoint, for rectangular beams, the best performance was demonstrated by the R-EP beam, which was able to recover all the strength mobilized before the occurrence of the first crack. For the beams with I geometry, after the first crack, it was still possible to mobilize an additional strength of 53% and 99%, for I-PU and I-EP beams, respectively, which corresponds to a considerable strength increase. In fact, as far as resistance is concerned, the performance of beams constituted by epoxy adhesive was substantially higher than that of beams made with polyurethane adhesive (1.37 and 3.95 times in the rectangular and I shaped beams, respectively). The strength presented by the R-PU beam was even lower than the average strength of the annealed glass beams, which may be due to glass flaws (unnoticeable before the test) and to the reduced degree of interaction provided by the adhesive. This difference in performance is essentially related with the different stiffness exhibited by polyurethane and epoxy adhesives and, in a certain way, with the adhesion problems (and construction difficulties – air bubbles) observed in the first adhesive.

As far as ductility is concerned, the fragile behaviour observed in annealed glass beams was not repeated in the GFRP reinforced beams – all composite beams showed a ductile behaviour after initial cracking, which, similarly to strength, varied with the reinforcement geometry and, especially, with the type of adhesive. As it had been predicted, the polyurethane adhesive, compared to the epoxy adhesive, allowed achieving a greater ductility – that was provided not only by the distribution of stresses between the two materials but, essentially, by means of the deformation capacity and reduced stiffness of the adhesive, which caused significant slippage between the two materials. It should be mentioned, however, that the achievement of greater ductility levels with the polyurethane adhesive has as a counterpart, namely the lower initial stiffness and post-cracking strength, when compared with the results obtained with the epoxy adhesive.

The numerical models developed simulated the serviceability behaviour of the glass beams and the glass-GFRP composite beams tested with good accuracy. The models allowed evaluating the failure stress of the glass and the distribution of stresses by the different materials that constitute the beams. It was proven that, if the adhesive does not present appropriate mechanical characteristics, particularly in what concerns its stiffness, the global behaviour of the composite beam can be compromised. The low stiffness of the polyurethane adhesive was the main cause for the less efficient behaviour of the composite beams in which it was used - the ultimate strength was particularly affected. In the future it would be interesting to model the post-cracking behaviour of the composite beams – models will have to consider the fracture mechanics of glass.

7. ACKNOWLEDGEMENTS

The author wishes to thank FCT and ICIST for funding the research and SIKA, Guardian and STEP companies for providing the adhesives, the glass and the GFRP profiles, respectively.

8. REFERENCES

- [1] Website: <http://www.servicehansen.com/>, visited in 2/8/2010.
- [2] Website: <http://www.archdaily.com/>, visited in 8/6/2010.
- [3] Louter, P.C., "Adhesively bonded reinforced glass beams", Heron, 2007, Vol. 52, p. 31-58.

- [4] Kreher, K.; Natterer, J. - "Timber-glass composite girders for a hotel in Switzerland", *Structural Engineering International*, 2004, Vol. 14, p. 149-151.
- [5] Veer, F., Gross, S., Hobbleman, G.J., Vredeling, M., Janssen, M.J.H.C., van den Berg, R. and Rijgersberg, H., "Spanning structures in glass", *In Proceedings of Glass Processing Days 2003*, Tampere, Finland, 2003.
- [6] Bos, F.P., Veer, F., Hobbleman, G.J. and Louter, P.C., "Stainless steel reinforced and post-tensioned glass beams", *In Proceedings of 12th International Conference on Experimental Mechanics*, Bari, Italy, 2004.
- [7] Louter, P.C., Belis, J., Bos, F.P., Veer, F. and Hobbleman, G., "Reinforced glass cantilever beams", *In Proceedings of Glass Processing Days 2005*, Tampere, Finland, 2005.
- [8] Louter, P.C., Veer, F. and Hobbleman, G., "Reinforcing glass, effects of reinforcement geometry and bonding technology", *In Proceedings of Glass Performance Days 2007*, Tampere, Finland, 2007.
- [9] European Committee for Standardization. "EN 1288-1: 2000. Glass in building – Determination of the bending strength of glass – Part 1: Fundamentals of testing glass; Part 3: Test with specimen supported at two points (four point bending)", CEN, Brussels, 2000.
- [10] Correia, J.R. – "GFRP pultruded profiles in civil engineering: hybrid solutions, bonded connections and fire behaviour", PhD Thesis, IST-UTL, 2008.
- [11] International Organization for Standardization. "ISO 527:1993. Plastics – Determination of the tensile properties – Part 1: General principles; Part 2: Test conditions for moulding and extrusion plastics", ISO, Genève, 1993.
- [12] Ansys® Academic Research, Release 11.0.
- [13] Veer, F., Zuidema, J. and Bos, F.P., "The strength and failure of glass in bending", *In Proceedings of Glass Processing Days 2005*, Tampere, Finland, 2005.